Modeling of Adsorption in UiO-66 and MOF-based Gas Sensor Arrays

by

Xin Wei

Undergraduate degree, Lamar University, 2019

Submitted to the Graduate Faculty of the

Swanson School of Engineering in partial fulfillment

of the requirements for the degree of

Master of Science in Chemical Engineering

University of Pittsburgh

2021

UNIVERSITY OF PITTSBURGH

SWANSON SCHOOL OF ENGINEERING

This thesis was presented

by

Xin Wei

It was defended on

March 26, 2021

and approved by

J. Karl Johnson, PhD, Professor, Department of Chemical & Petroleum Engineering

Christopher E. Wilmer, PhD, Associate Professor, Department of Chemical & Petroleum Engineering

John A. Keith, PhD, Associate Professor, Department of Chemical & Petroleum Engineering
Thesis Advisors: J. Karl Johnson and Christopher E. Wilmer

Modeling of Adsorption in UiO-66 and MOF-based Gas Sensor Arrays

Xin Wei, MS

University of Pittsburgh, 2021

Metal-Organic Frameworks (MOFs) have attracted significant interest for adsorption due to their high degree of tailorability and large specific surface areas. The combination of tailorability and well-defined crystalline pores makes MOFs very promising candidates for highly selective adsorption.

In this study, we explored the properties and applications of MOFs in three areas. Firstly, we studied how adsorption correlates with the number and types of defects. Molecular-level modeling of adsorption and diffusion in MOFs almost always relies on models of MOFs that are defect-free (pristine). However, all real MOFs have defects, which affect adsorption by changing the environment of pores within the MOFs. A fundamental understanding of how defects impact adsorption is important for identifying the limits of the performance of real materials, developing improved design rules for new improved materials, and predicting and maximizing utilization of the material. We initially consider UiO-66 with different levels of missing linker defects. The structures of the generated defective MOFs were optimized using periodic density functional theory with the CP2K simulation package. Adsorption isotherms were generated by carrying out grand canonical Monte Carlo (GCMC) simulations in RASPA. We also investigated the effect of different adsorbate-adsorbent charge schemes by comparing isotherms with no framework charges and atomic charges calculated using DDEC6 and EQEQ methods.

Secondly, we generated new forcefields using the QuickFF formalism for both pristine UiO-66 and 17% defective UiO-66 to facilitate simulation of flexible structures. Bulk modulus

calculations, relaxation, and NVT simulations were used to test the validity of the newly developed potentials.

Thirdly, we studied one use of MOFs for developing an electronic nose, a device intended to identify the composition of complex gas mixtures. We modified and improved the previously developed algorithm by applying Henry's law coefficients and moving CO_2 from the trace gas category to background gas. Applying Henry's law coefficient enables the prediction without performing GCMC simulations of every specific composition combination. Treating CO_2 as a background gas enlarged the library of MOFs we can use in the electronic nose by freeing it from the restrictions of Henry's coefficient of CO_2.

Table of Contents

List of Tables

List of Figures

Preface

Collaboration with Yao An, Amanda Morris, Bradley Gibbons, Trenton M. Tovar, John J. Mahle, Christopher J. Karwacki, and Yue Wu

The Defense Threat Reduction Agency (DTRA) for funding

Center Research Computing (CRC)

DTRA HDTRA1-16-1-0044

Army Research Office W911NF-19-2-0187

Priyanka Shukla

Brian Day

Johnson group – University of Pittsburgh

Wilmer group – University of Pittsburgh

1.0 Modeling of Adsorption in UiO-66

1.1 Introduction

Metal-organic frameworks (MOFs) have drawn growing interest in the adsorption and degradation of chemical warfare agents (CWAs) and other hazardous industrial compounds because they have a high-level degree of tailorability and the highest surface areas compared to other typical porous materials. UiO-66 is among the most thoroughly investigated MOFs for this purpose. The adsorption of isopropyl alcohol (IPA) and nitrogen in UiO-66 with differing defect amounts is the subject of this research. We selected IPA and nitrogen as adsorbates since they are small particles that can be analyzed experimentally and have similarities to different CWAs.

MOFs have two main building blocks: organic linkers and inorganic secondary building units (SBUs, also known as nodes). Figure 1 shows the arrangement of UiO-66. It is a periodic structure composed of twelve 1,4-benzodicarboxylic acid linkers per node and [Zr6O4(OH)4] nodes. The periodic structure of UiO-66 is seen in Figure 1b. The dark blue sphere represents the octahedral pore, while the light blue sphere represents the tetrahedral pore; both may be used for gas storage.

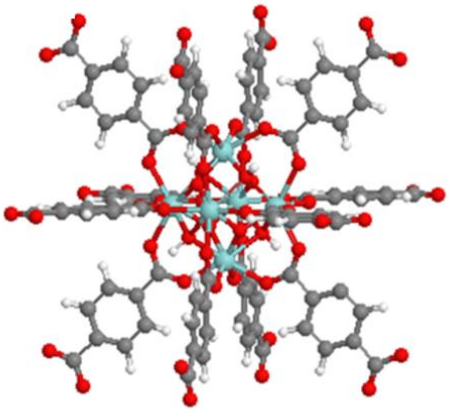

Figure 1a One Unit Cell of UiO-66

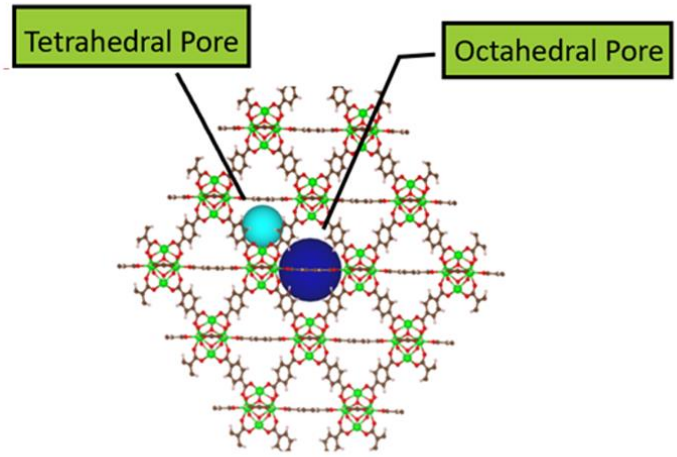

Figure 1b Periodic Structure of UiO-66

Present molecular-level simulation of adsorption and diffusion in MOFs nearly always depends on defect-free MOF models (pristine). Under standard synthesis conditions, defects are naturally present in UiO-66 frameworks and affect adsorption by modifying the atmosphere of pores within the MOFs.[1, 2] A thorough understanding of just how defects impair adsorption is crucial for evaluating the limits of real-world material efficiency, designing better design guidelines for new materials, and improving material use. Besides, missing linkers are needed for chemical warfare agents to react.

In UiO-66, both missing linker and missing cluster defects may occur and tend to result in stable frameworks.[3, 4] Figure 2 shows the distinction between pristine UiO-66, defective UiO-66 with missing linkers, and defective UiO-66 with missing clusters. Also, the most common defect is missing linkers. It can be tuned by changing the modulators during synthesis.[5, 6]

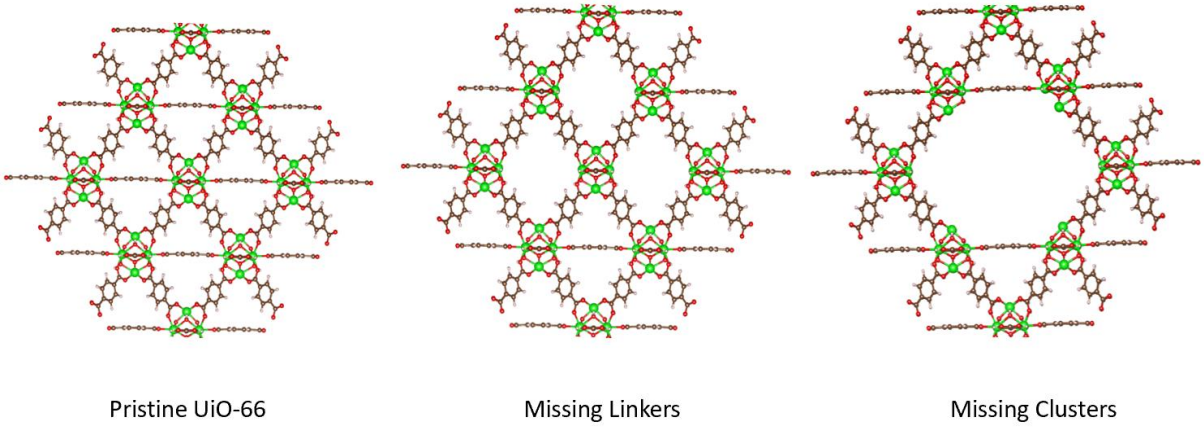

Figure 2 Different Types of Defects in UiO-66

1.2 Method

1.2.1 Generate Models of Defective MOFs

Defective structures are formed by removing varying numbers of 1,4-benzene dicarboxylate (BDC) linkers from pristine UiO-66. By removing one organic linker, four open metal sites are created. For each missing linker, two capping groups must be applied to open metal sites to maintain charge neutrality. Hydroxyl and formate are two capping groups investigated in this research. Virginia Tech experiments show that formate is by far the most possible capping group.[7] DFT calculations in CP2K were used to optimize the geometries of the developed structures.

With each deleting linker, there is only one way to add formate and two ways to add hydroxyl group. Figure 3 shows various methods of capping the open metal sites. Figure 3a shows

an entire organic linker bound to four Zr atoms. Figure 3b represents a missing linker structure capped by formate groups. Figures 3c and 3d show two alternatives to incorporating hydroxyl groups to neutralize the one missing linker structure. The two methods of adding hydroxyl groups are known as trans and cis substitution and are shown separately in figures 3c and 3d. Trans replacement has the lowest energy arrangement, which can be explained by electrostatic and steric effects.[8] In this analysis, we modeled defective structures with 4%, 8%, 17%, and 33% defect levels. One missing linker was removed per primitive cell to create UiO-66 with 8% defects. The primitive cell for UiO-66 with 17 % and 33 % defects was extended to 2 by 1 by 1 and 2 by 2 by 1 before removing one linker. Two missing linkers were removed per primitive cell to create the structure with 4% defects.

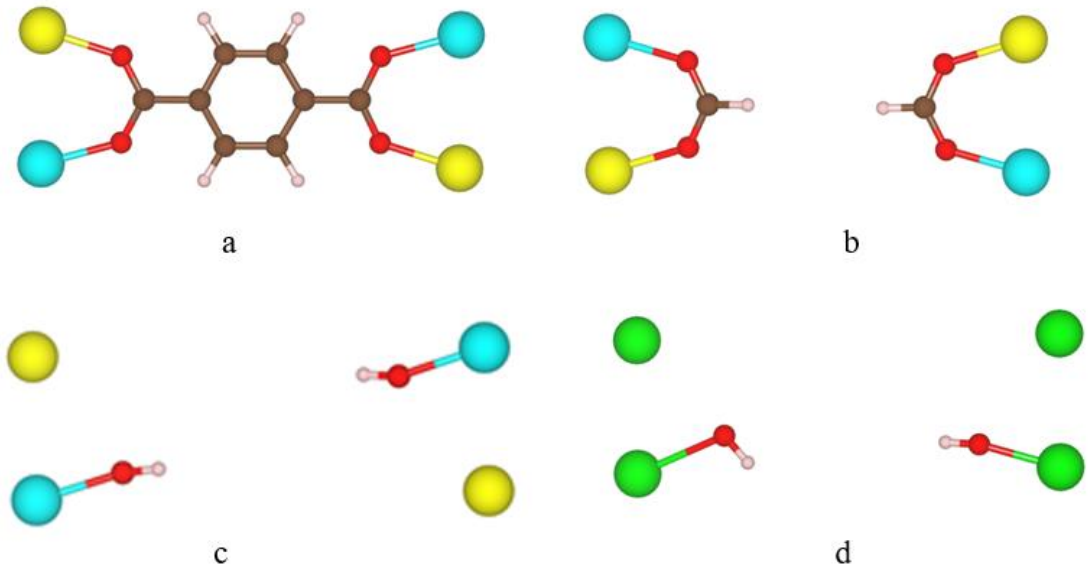

Figure 3 Different Ways of Adding Hydroxyl Groups

Figure 4 illustrates two symmetrical inequivalent ways for removing two linkers from an UiO-66 primitive cell. In the periodic structure, two half linkers defined by lines of the same color will join to form a whole link, which should also be removed together when generating the structures. The deletion of linkers is shown by red lines. The energies for various structures of UiO-66 with 4% defects were determined using energy minimization calculations in CP2K and are shown in table 1. Numbers 1 and 2 reflect how the linkers referring to structures 1 and 2 in figure 4 are removed. The letters y, g, and b represent the locations of the hydroxide groups, which correspond to the colored Zr in figure 4. Since Structure 1 has the lowest energy, it was used in the adsorption simulations.

Final structures were obtained by running geometry optimization simulations using CP2K.

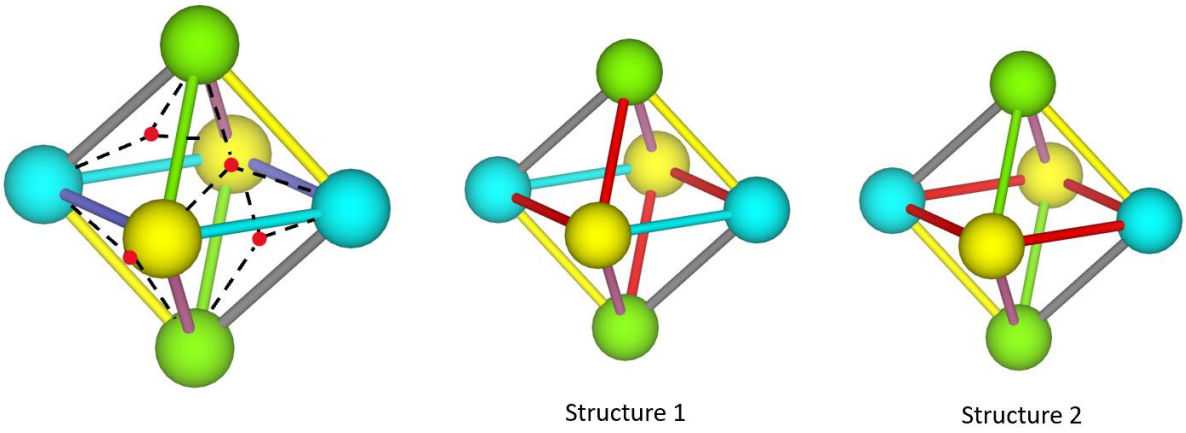

Figure 4 Different Ways to Remove Two Linkers per Primitive Cell for UiO-66

Table 1 Energies for Different Structures of UiO-66 with 4% Defects

	1_yb	1_yy	1_bg	1_by	2_by	2_bb
a.u.	-929.5	-929.42	-929.45	-929.5	-929.46	-929.43
kJ/mol	-2440389.0	-2440196.00	-2440262.00	-2440394.0	-2440295.00	-2440219.00

1.2.2 Charge Calculations

In this analysis, atom-centered charges measured in Chargemol using the density-derived electrostatic and chemical (DDEC6) approach were used.[9-12] CP2K was used to generate the density file required for the calculation.[9] EQEQ method has also been tested.[13]

1.2.3 LJ Parameters and Forcefield Selection

Priyanka Shukla in Dr. Karl Johnson's group explored the effect of different potentials for both framework and adsorbates, like UFF, DREIDING, SKS, and OPLS; findings indicate that the saturation loading and general shapes using all the potentials agree. We choose the modified UFF potential with the LJ parameters from the TraPPE potential, $\sigma_H = \varepsilon_H = 0$, $\sigma_O = 0.302$ nm, and $\varepsilon_O =$ 93 K, instead of the UFF potential for μ_3-OH and added OH to capture hydron bonding.

Initially, we used Lennard-Jones potentials from the UFF force field for the system. However, the Lennard-Jones potentials from UFF were unable to capture the hydrogen bonding because the LJ radius, as seen in figure 5a, is too large in contrast to the standard length of a

hydrogen bond, which is usually less than 2 Å. Both AIMD and diffusion simulations demonstrated that hydrogen bonds formed between the IPAs and the framework.

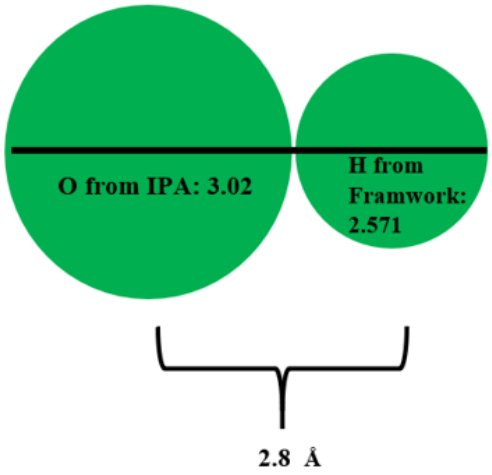

Figure 5a Standard UFF Potential

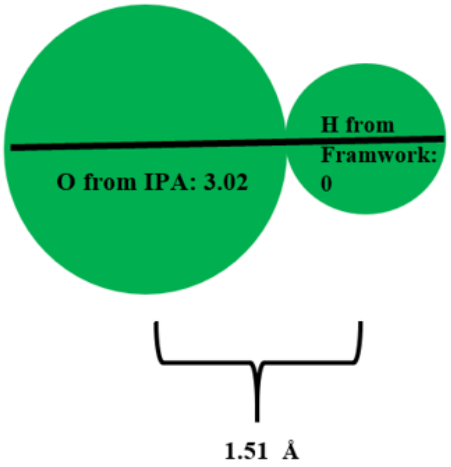

Figure 5b Modified UFF Potential

1.2.4 Adsorption Isotherms Computed using RASPA

The GCMC simulation in RASPA was used to model adsorption isotherms for IPA at 291K and N_2 at 77K, which have been the temperatures used by the experimental collaborator, in pristine UiO-66 and UiO-66 with 4%, 8%, 17%, and 33% defect levels. For pristine UiO-66 and defective structures with 17 % and 33% defects, a 3x3x3 unit cell has been used as a simulation cell. A 2x2x3 supercell has been used for defect levels of 4% and 8%. The Helium void fractions were

calculated using RASPA as well, and they are 0.47508, 0.509683, 0.513973, 0.533021, and 0.58203 for pristine and defective UiO-66s with 4%, 8%, 17%, and 33% defect levels, respectively. For swap, reinsertion, rotation, and translation odds, the relative probabilities were 2:1:1:1.

1.2.5 Method for Counting Hydrogen Bonds

To track the number of adsorbates bonded to μ3-OH and added OH separately, a python code was written. The script ran over all of the IPAs and counted how many IPA molecules are hydrogen-bonded to the added OH groups, μ3-OH groups, and both of them.

1.3 Result and Discussion

1.3.1 Pristine MOF

To validate the accuracy of our GCMC simulations, isotherms for N_2 at 77 K and IPA at 291 K were compared to experimental results. Figures 6 and 7 show our isotherms and the comparison with experiments. We greatly underestimate the loading of IPA for relative pressures above 0.02 and normally overestimate the volume adsorbed at lower pressures for all potentials measured. In comparison, our simulations overestimate N_2 loading for all pressures. The inaccuracy of the potential models used, level of defects or capping groups are our hypotheses for the inconsistency within the simulation and experiments for adsorption of IPA. Our experimental collaborators proposed that defects could be introduced to the experimental sample during

transference and reactivation (samples were shipped from Virginia Tech, whereas the N_2 isotherms were measured to the University of North Carolina, where the NMR measurements were made).[7] The residual solvent in MOF is our best explanation for the difference between simulation and experimental results for N_2.

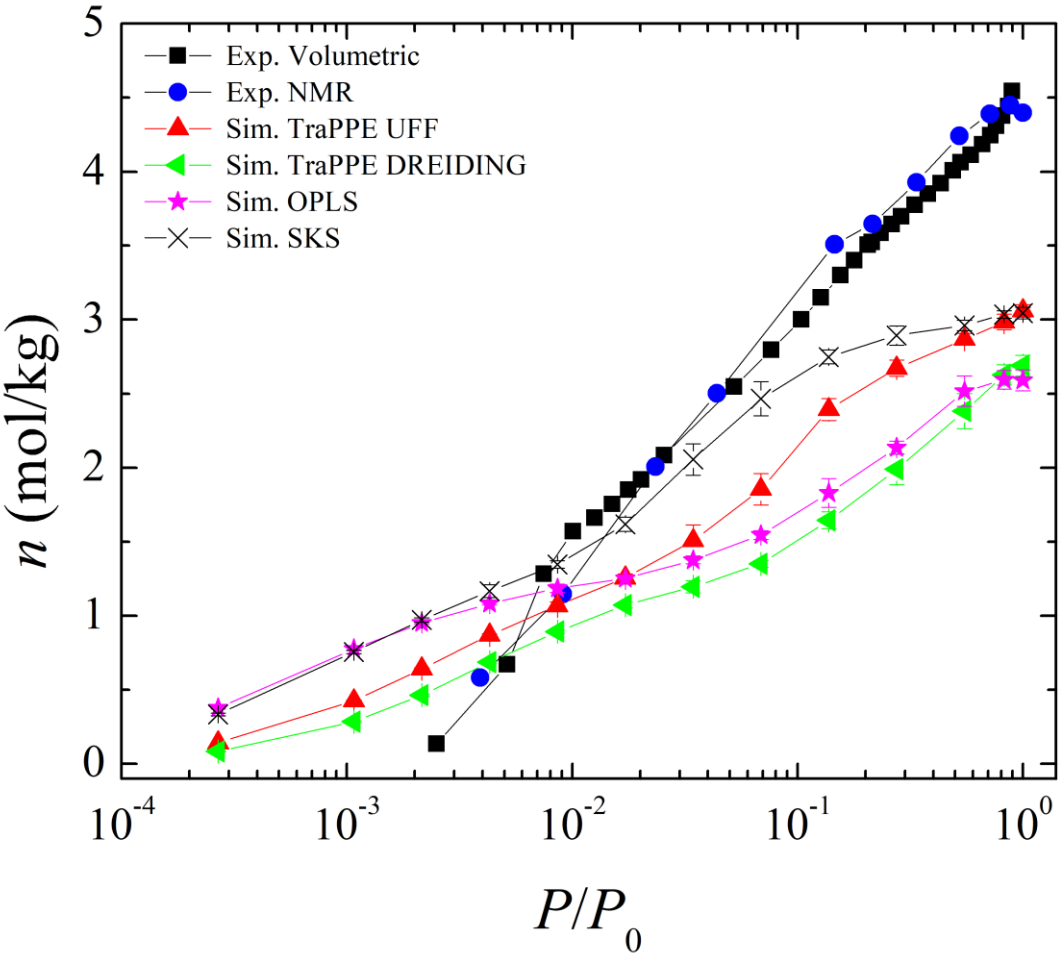

Figure 6 Isotherms for IPA at 291 K

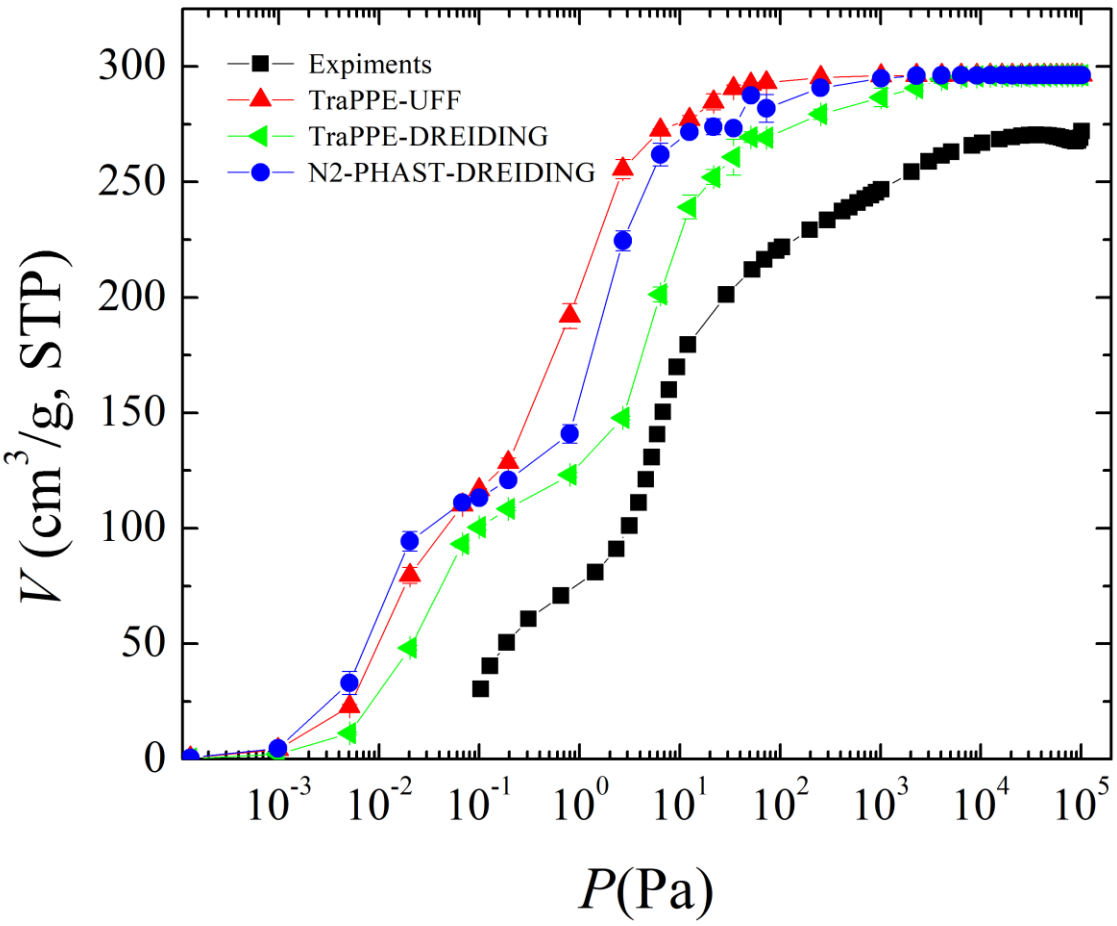

Figure 7 Isotherms for N_2 at 77 K

1.3.2 Defective MOF

1.3.2.1 OH Capped Defective Structures

GCMC calculations using standard UFF and DREIDING LJ parameters effectively prevent hydrogen bonding with IPA. However, the Langmuir adsorption study and NMR findings from our collaborator's experiments indicate that hydrogen bonds existed.[7] To further illustrate the presence of hydrogen bonding, we ran AIMD simulations to explore the possible binding sites of

the adsorbates. AIMD simulations for IPA in both pristine and defective UiO-66 indicate hydrogen bonding between IPAs and framework. Figure 8 shows a snapshot from the DFT calculations in which IPA is hydrogen-bonded to both μ3-OH and added OH.

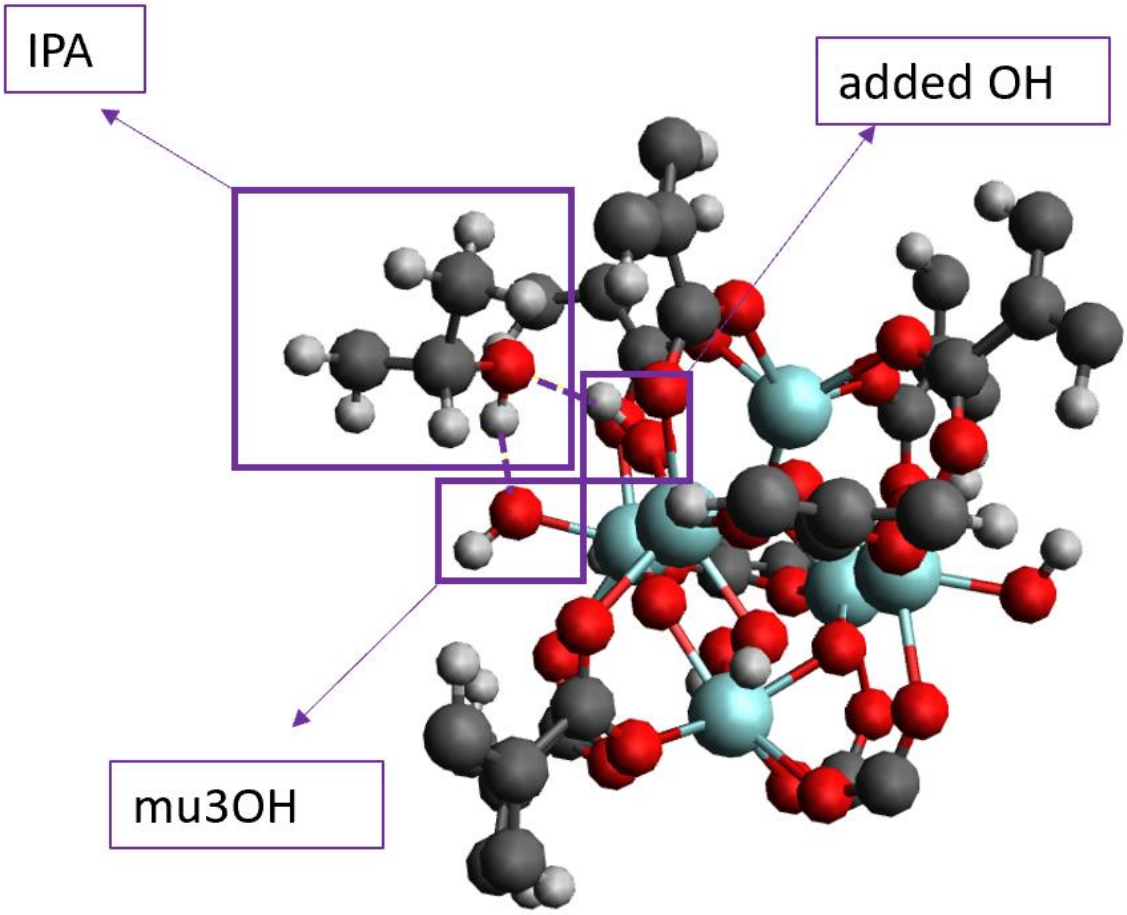

Figure 8 One Snapshot from the DFT Calculation

Figures 9 and 10 provide a comparison of IPA isotherms using the normal UFF potential and the adjusted UFF potential, which replaces the O and H Lennard-Jones parameters for the μ3-OH and added OH with TraPPE potential. Figure 9 reveals that hydrogen bonding has little effect on IPA adsorption in pristine UiO-66. By counting hydrogen bonds formed between added OH and μ3-OH, we found that most of IPAs are hydrogen-bonded to added OH. And that explained why modified potential has little effect on pristine UiO-66. Figure 10 reveals that hydrogen bonding has an effect on IPA adsorption in defective UiO-66 at low pressures but not at saturation pressure. At saturation pressure, the adsorption is determined by void volumes.

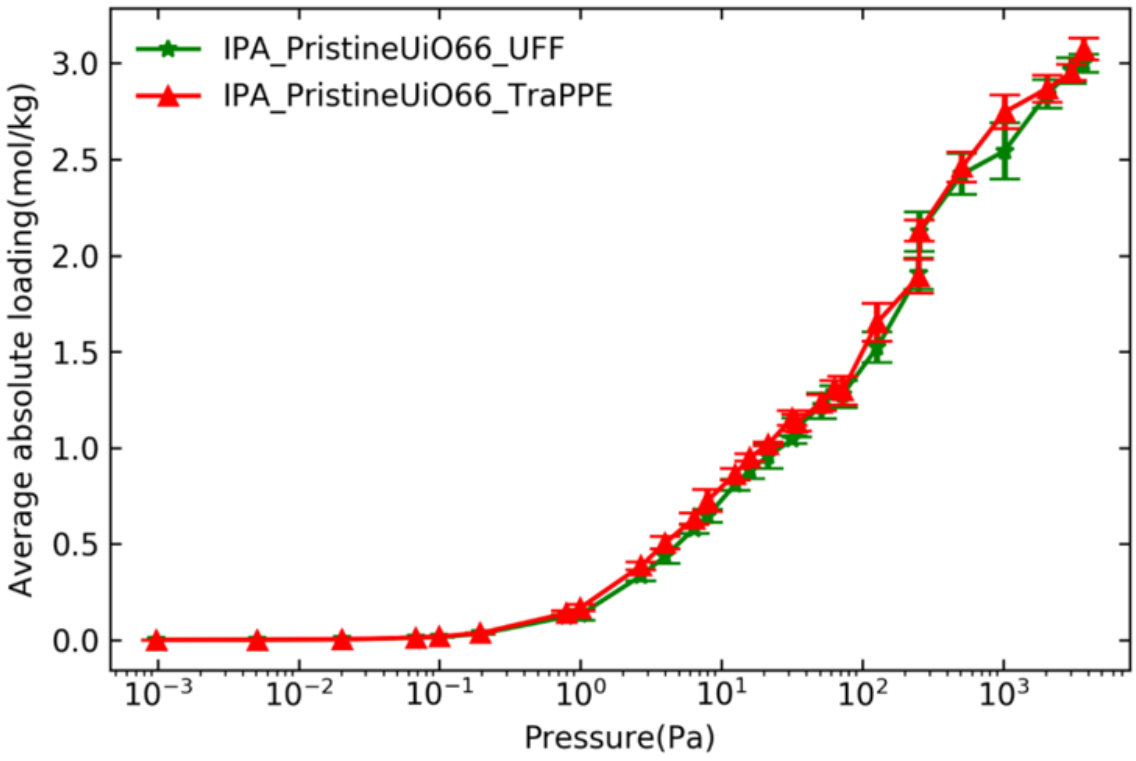

Figure 9 Comparison between Isotherms of IPA using Standard UFF Potential and the Modified UFF Potential for Pristine UiO-66

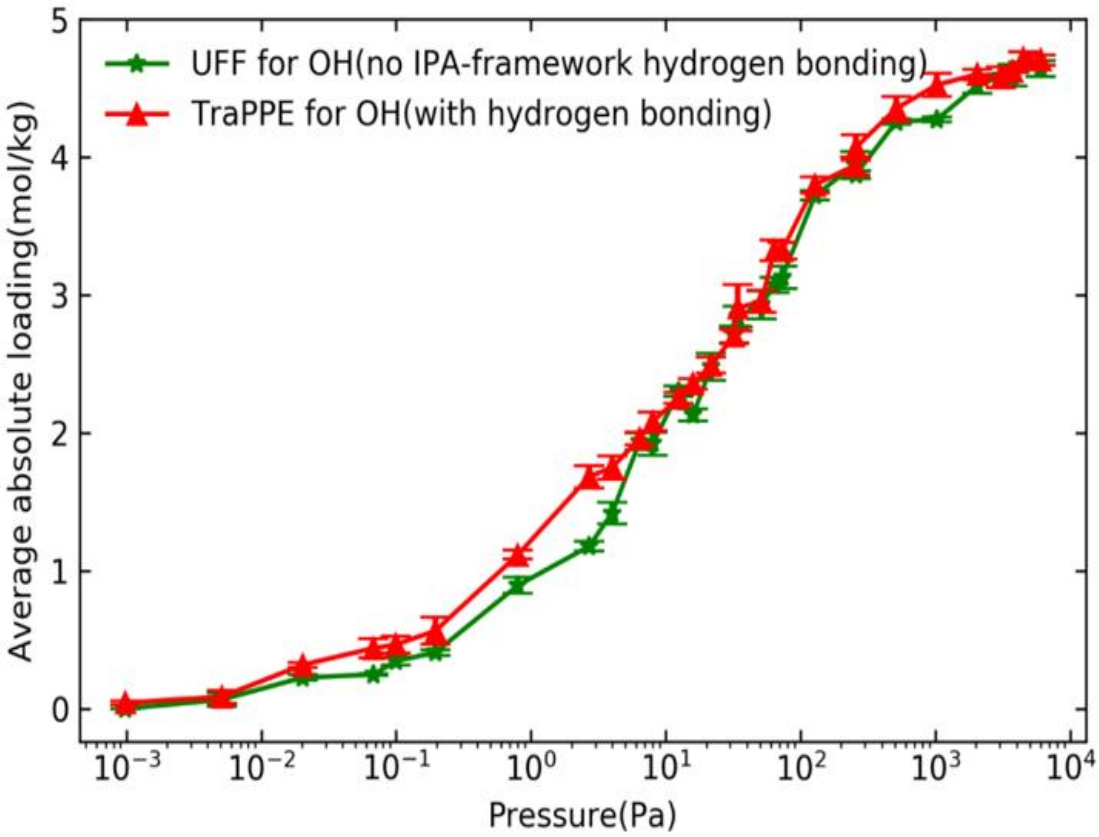

Figure 10 Comparison between Isotherms of IPA using Standard UFF Potential and the Modified UFF Potential for Defective UiO-66

Figure 11 shows IPA isotherms for UiO-66 with differing amounts of defects. Adsorption increases at lower pressures as the defect level increases because the additional OH groups provide new binding sites for IPA. Adsorption increases at higher pressures as the defect level increases due to the increased void space.

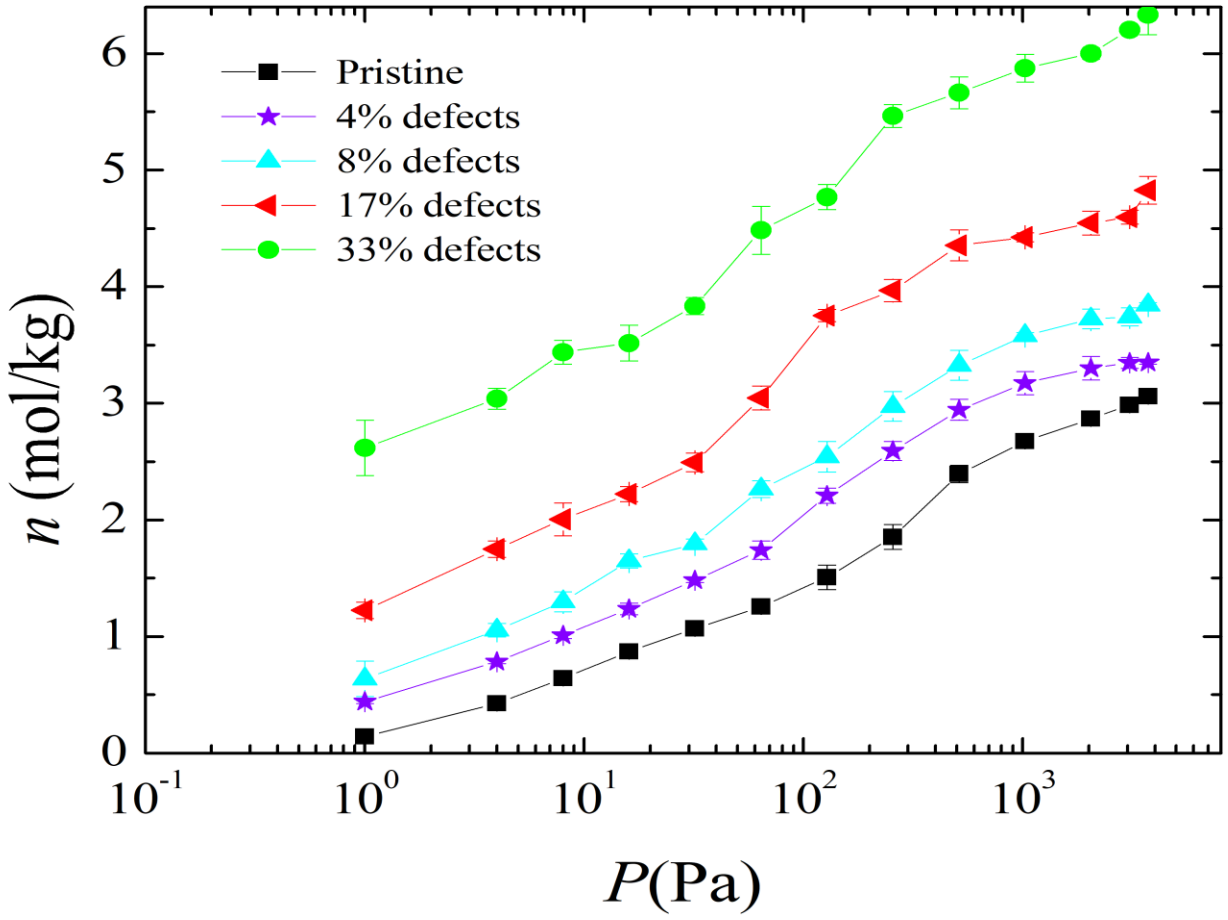

Figure 11 Isotherms of IPA in Defective UiO-66

Figure 12 shows the contrast of IPA isotherms between structure 1 and structure 2 shown in figure 4. At lower pressures, there is indeed a significant difference. We guess that the low energy structure's configuration of OH groups prevents hydrogen bonding between IPA and the framework. In the future, low energy structures with different OH configurations will be tested.

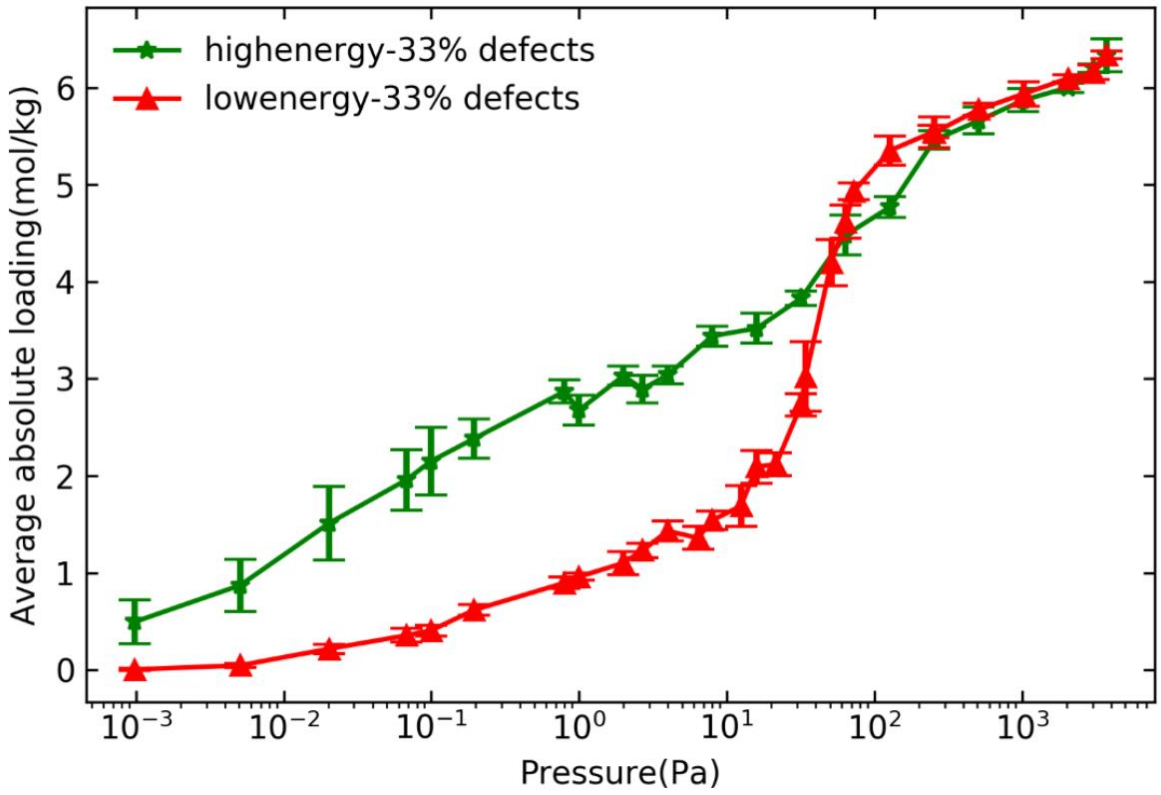

Figure 12 Isotherms of IPA in UiO-66 with 33% Levels of Defect

Figure 13 shows a contrast of isotherms of pristine UiO-66 and 17% defective UiO-66 which is capped by OH groups. We discovered that the defective structure has a greater potential at both low and high pressures by contrasting the isotherms. One potential explanation is that the added OH groups provide new binding sites for IPA at lower pressures and missing linkers increase the void fraction.

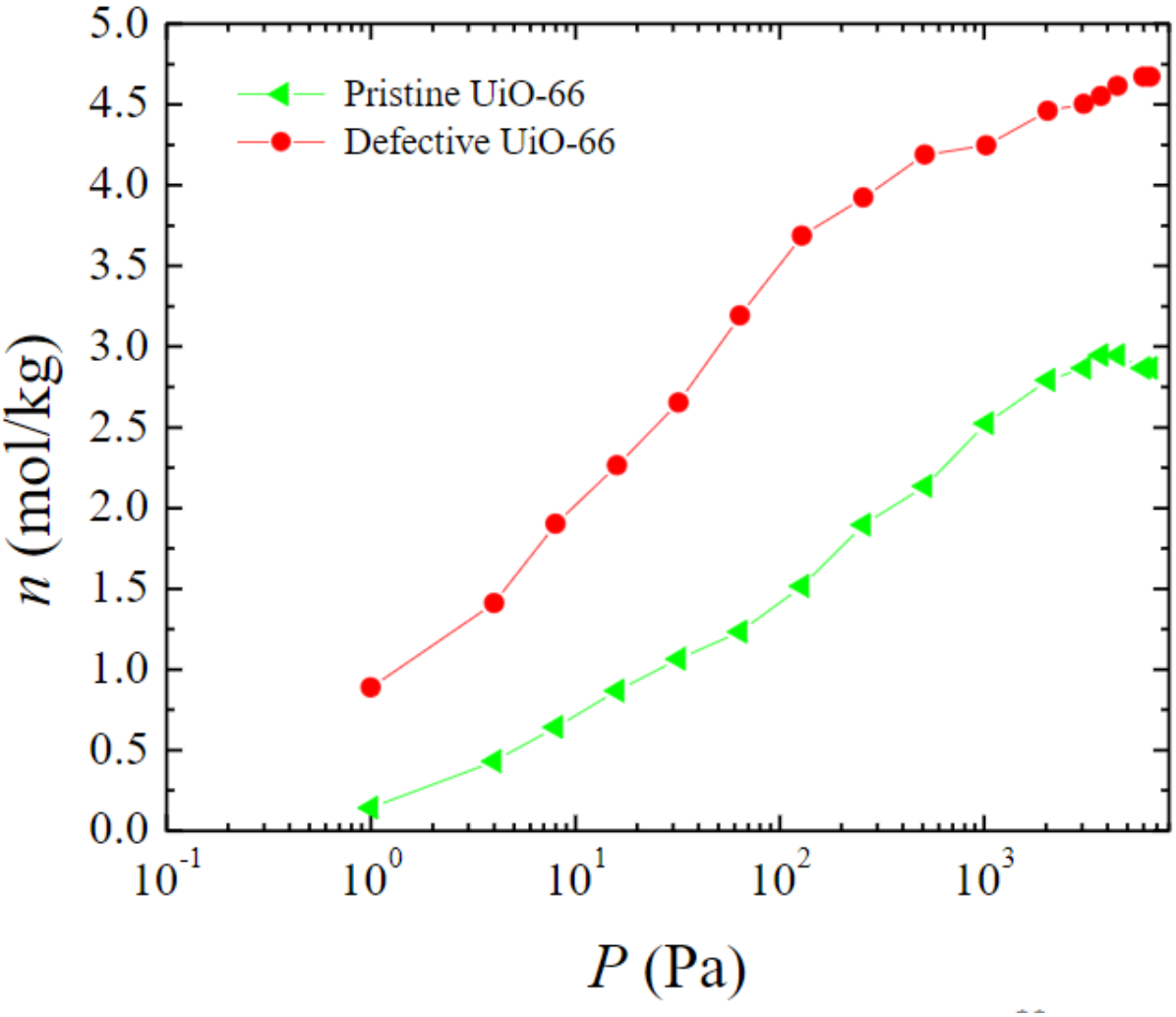

Figure 13 Comparison between Isotherms of Pristine UiO-66 and 17% Defective UiO-66 Capped by OH Groups

1.3.2.2 Formate Capped Defective Structures

Experiment findings reveal that the defective samples have a lower capacity at relatively low pressures and a higher capacity at relatively higher pressures, which contradicts our simulated results. And this variation may be due to the capping groups. According to the literature, the

capping group may be OH, formate, acetate, or other capping groups.[14] Experiments at Virginia Tech have also shown that formate is by far the most likely capping group. Based on that, we generated structures capped with formate and ran Grand canonical Monte Carlo (GCMC) simulations to further demonstrate this hypothesis.

Isotherms are plotted alongside the experimental results in Figure 14. At lower pressures, there is a substantial disparity between those two capping groups for structures with a 33% defective level and structures with a 17% defective level. There isn't much of a distinction with other structures. This phenomenon could be explained by that capping groups will make more impact on structures with higher defect levels at lower pressures. For higher pressures, adsorptions are determined by void spaces. And for structures with lower defect levels, the ratio of capping groups to other binding sites is not high enough to make an observable impact by only changing the capping group.

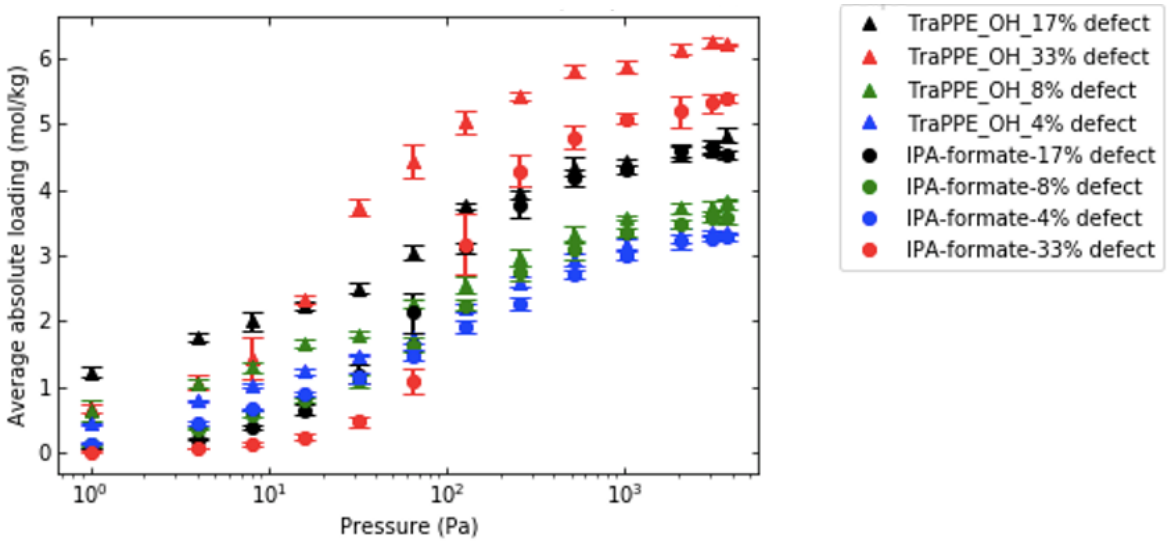

Figure 14 IPA Adsorption in All Level of Defects Capped with Formate Groups and Added OH Groups

As a function of pressure, we calculated the fractions of IPA molecules that are hydrogen-bonded to either 3-OH or added OH groups. Figure 15 shows the results. As expected, as pressure increases, the fraction of IPA molecules that are hydrogen-bonded to the framework decreases since void fraction, instead of binding sites, dominates the loadings at higher pressures.

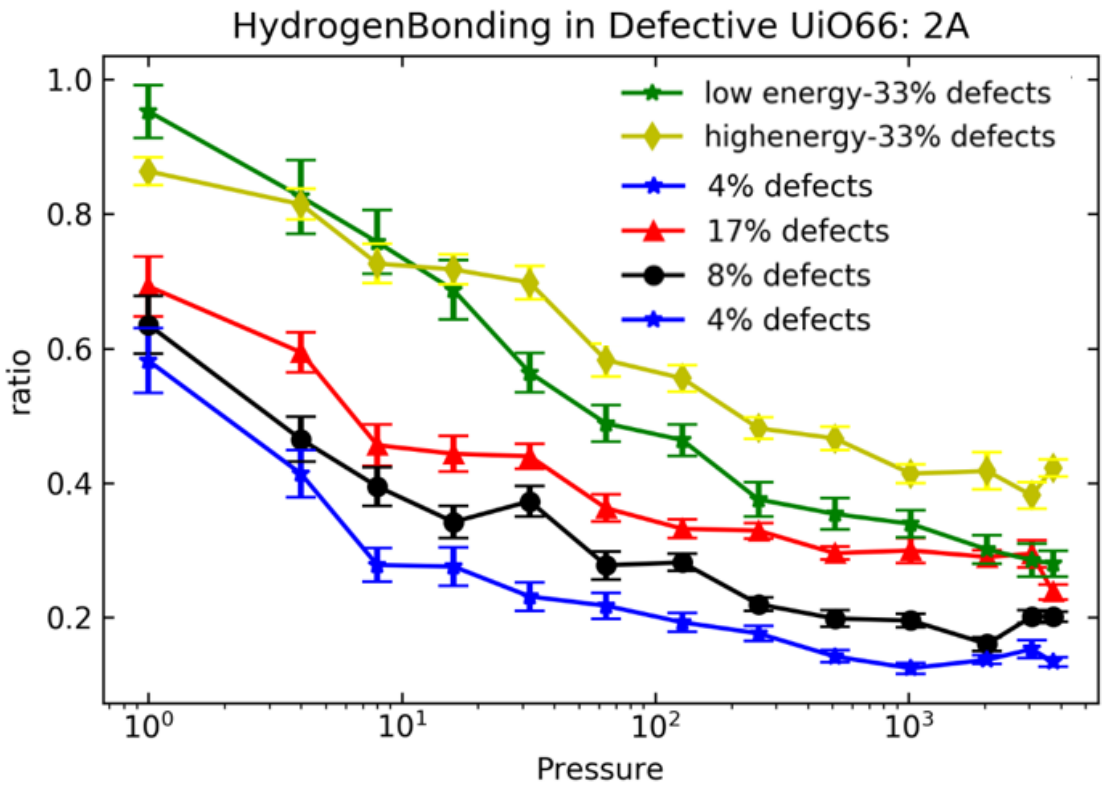

Figure 15 Fraction of IPA Molecules that are Hydrogen-Bonded

2.0 Forcefield Development using QuickFF

2.1 Introduction

QuickFF is a Python package developed at the Centre for Molecular Modeling (CMM) that uses ab initio calculations to produce precise force fields.[15]

The previous research demonstrated the importance of system flexibility for obtaining physically realistic values of diffusivities for acetone and similar-sized polar molecules in UiO-66.[16] The problem with the previously used Boyd et al. potential is that during geometry relaxation, the μ3-O atoms of the SBU moved from their DFT-optimized positions to unphysical positions. Figure 16 shows the before and after images of SBUs that have undergone geometry optimization. Some μ3-O atoms collapse into the SBU and merged with other μ3-O atoms. This highlights the importance of developing an accurate forcefield for UiO-66 that could be used in dynamic simulations.[16]

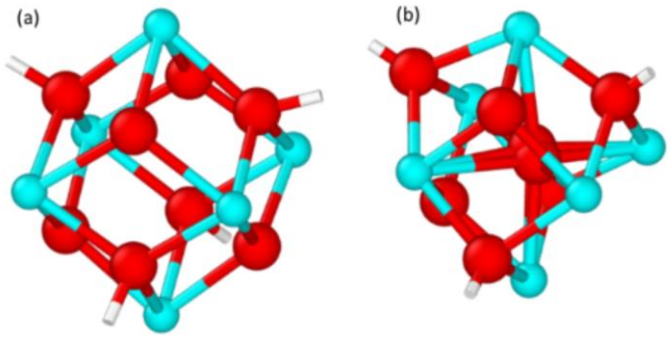

Figure 16 Before and after Pictures of the SBU that go through Geometry Relaxation using QuickFF Potential

The ultimate goal of this part is to produce flexible framework potentials for UiO-66 and related materials with various levels of missing linker defects. In the future, we want to use these potentials to simulate the diffusion of molecules through the defective UiO-66 as a function of the number of missed linker defects. The developed force field consists of three parts: an electrostatic contribution, a van der Waals contribution, and a covalent contribution. The final goal of QuickFF is to generate covalent contribution parameters that are as precise as possible in reproducing the ab initio geometry and matrix measured in the frequency calculation.[17]

2.2 Method

In QuickFF, there are two ways to generate a force field: cluster-based models and periodic models. The original QuickFF protocol relied on *ab initio* data generated from small cluster models, which were cut from the periodic structure. Since such a procedure is far from trivial, we chose to use periodic models in this study.[18] The periodic structures for pristine and defective MOFs were prepared in Avogadro and optimized using CP2K.

QuickFF implements a three-step procedure for generating a force field. The methodology's first two steps are intended to reduce associations between force field parameters. The parameters were refined in the final step by regenerating the ab initio Hessian matrix created by frequency calculations using the force field parameters.[17]

To produce the potential, three input files were used: a geometry and hessian matrix file, a charge file, and a van der Waals file. The Geometry and hessian matrix file is an XML file generated by the Vienna Ab initio Simulation Package (VASP) during frequency calculations.

Charges were calculated in Chargemol using the DDEC6 method. The charges obtained from the DDEC6 system are point charges.[9-12] We used the DDEC6 approach to maintain consistency with previous Lammps simulations. To maintain continuity, we used the same Lennard Jones potential, TraPPE for μ3OH, and added OH; UFF for all other framework atoms as we did in the previous adsorption simulations. We also excluded all nonbonded interactions, Lennard-Jones, and Coulombic interactions, between atoms that are three bonds or less apart since the interactions between those atoms were already defined by covalent bond potentials. The created covalent contribution is made up of bonds, bends, out-of-plane distances, dihedral, and cross terms. Cross terms are used to account for certain interactions that affect others.

2.3 Results and Discussion

Bulk modulus is a measure of resistance to compression. It is defined as the ratio of pressure stress to volumetric strain. Bulk modulus is one of the properties that can be used to validate the developed potential.

Figure 17 shows the curve fitting of the Birch-Murnaghan equation for pristine UiO-66 using energies calculated using VASP. 0.96, 0.97, 0.98, 1.0, 1.02,1.03, and 1.04 are the lattice scaling values used. Figure 18 shows the fitting of the Birch-Murnaghan equation for pristine UiO-66 using energies determined using the developed QuickFF potential. The minima of those two parabolas are the bulk modulus and equilibrium volumes. The bulk modulus calculated by DFT is 32.477 GPa, while the bulk modulus calculated by QuickFF potential is 34.487 GPa. These two figures are almost identical.

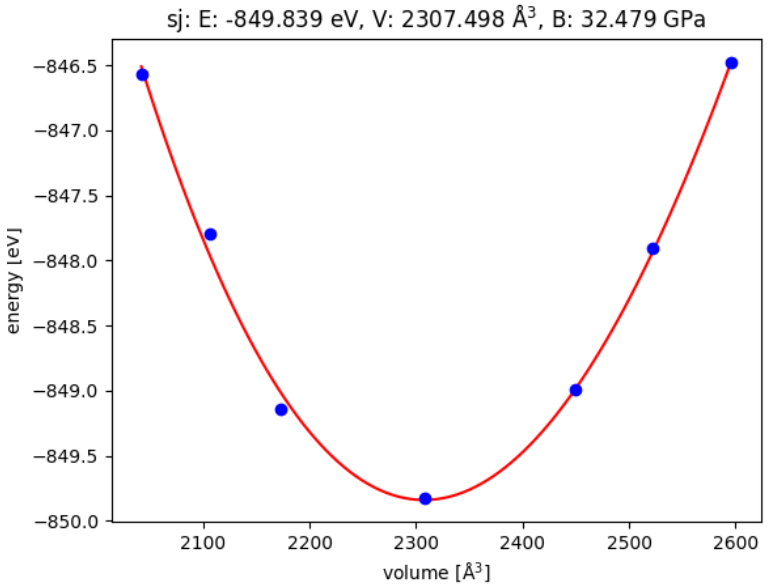

Figure 17 Curve Fitting of the Birch-Murnaghan Equation for Pristine UiO-66 using Energies Calculated by VASP

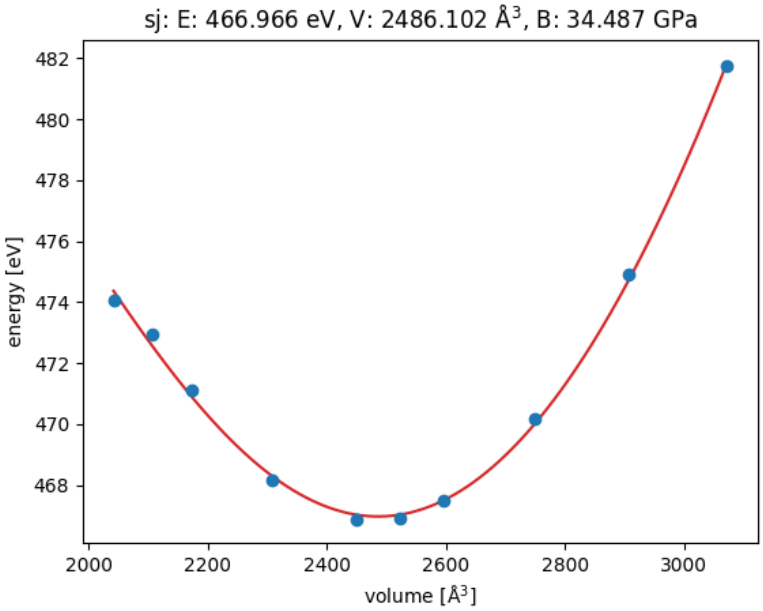

Figure 18 Curve Fitting of the Birch-Murnaghan Equation for Pristine UiO-66 using Energies Calculated using Developed QuickFF Potential

To validate the built potential, energy minimization and NVT were simulated too. During the relaxation, the SBU for both the pristine and defective structure extended marginally by μ3OH shifting away from the SBU. The organic linkers have a small rotation for pristine structure. There is no observable movement on organic linkers in defective structures.

2.4 Future Work

We can validate the built forcefield by employing additional techniques such as measuring diffusion coefficients and conducting molecular dynamic simulations. Besides, we can build QuickFF potential for systems with varying degrees of defects.

3.0 MOF-based Gas Sensor Arrays

3.1 Introduction

Gas sensor arrays, often known as electronic noses, are portable devices designed to detect odors or flavors by mimicking biological noses. Because of their large surface area and chemical and structural tunability, metal-organic structures (MOFs) have emerged as attractive materials for electronic noses.[19]

Brian Day, a graduate student from Dr. Chris Wilmer's group, developed a computational methodology for screening large amounts of metal-organic frameworks (MOFs) to design an electronic nose for disease detection. I focused on running raspa simulations to obtain composition results, as well as calculating Henry's coefficient and analyzing the data.

Figure 19 illustrates the function of the mechanical nose. Once the breath hits the surface acoustic wave (SAW), a sensor that can measure changes in mass, the mass of adsorbed mass will be detected. MOFs are assumed to be deposited on the SAW as thin films. As the SAW detects a mass change, it sends out signals that reflect the mass change for data analysis. During the data analysis process, the developed computational methodology converts mass value to composition value.[20] Since the concentration of such gases is a significant indicator for many diseases, like ammonia for kidney disease and acetone for liver disease, the electronic nose has a promising future in disease diagnosis.

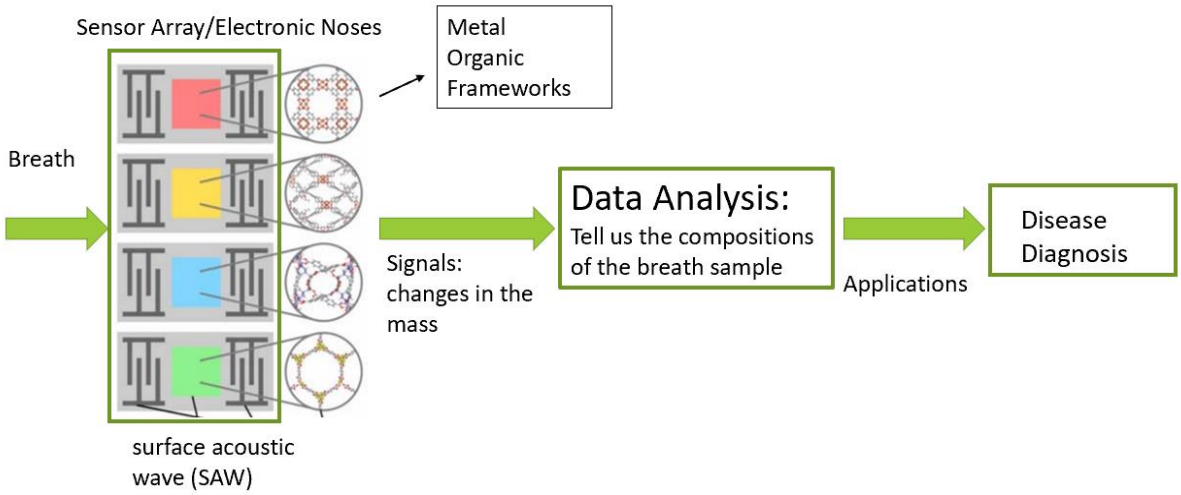

Figure 19 Schematic Diagram of Electronic Nose

The end product of data processing is a library of data on adsorbed masses as a function of composition. The idea is to compare the detected mass from the actual sensor device with the mass library and assign a probability to each composition in the data space.

The previous approach has a significant bottleneck in that we must run simulations for each composition that we'd like to predict. When we start looking at complicated gas mixtures, the numerical overhead becomes explosive, and screening all of those arrays becomes impossible. As a result, we used something similar to Henry's law constant, which essentially qualifies a linear relationship between the amounts of gas adsorbed and its concentration in the bulk. Previously, N_2 and O_2 were treated as background gases, but CO_2 was considered as a trace gas. However, treating CO_2 as a trace gas reduced the number of MOFs eligible for use in the design of the electrical nose. Since CO_2 has comparatively higher concentrations, certain MOFs must be discarded because they do not have the appropriate Henry's regime for all gases. We now consider CO_2 to be a background

gas. It enables us to create more adaptable sensor arrays. And Henry's law constant would be a function of the CO_2 compositions.

Figure 20 illustrates the modified prediction algorithm which is developed by Brian Day: 1. Create a grid of points of known compositions which likely contain the composition of detected breath. 2. Convert compositions to mass using the Henry's Law constant. 3. Compare data from mass space to experimental mass. 4. Assign a probability to all compositions based on the comparison in step 3. 5. Filter out low probability compositions. 6. Subdivide high probability regions of space into new compositions. 7. Repeat the whole process until converged.

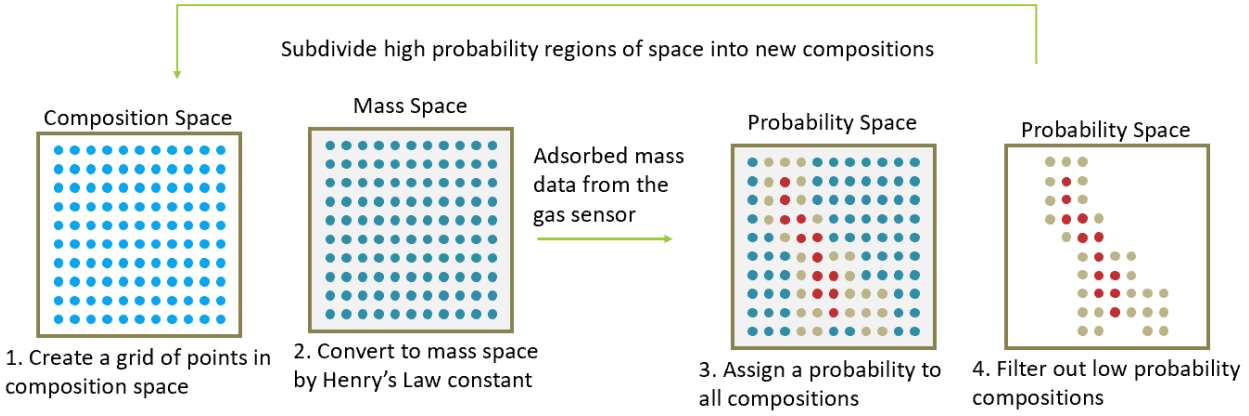

Figure 20 Prediction Algorithm of Electronic Nose

3.2 RASPA Simulations and Data Analysis

We investigated a series of gas mixtures containing CO_2, O_2, N_2, and acetone to model acetone in air. The CO_2 and trace gas compositions ranged from 0% to 5%, each in 1% increments, with the remainder being N_2 and O_2 in a 4:1 ratio.

The RASPA simulations were performed at a temperature of 298 K and a pressure of 1 bar, which matched the ambient conditions. 5000 equilibration cycles and 20000 production cycles were used for all simulations. To get a diverse representation of surface areas and void fractions, 9 MOFs were chosen from the CoRE MOF database. The EQEQ approach was used to assign charges to framework atoms to model electrostatic interactions, which are crucial for correctly predicting CO_2 and N_2 adsorption.[13] TraPPE potential was used for both framework and adsorbate. Python code developed by Brian Day was used to calculate Henry's law constant.

3.3 Result and Discussion

Nine MOFs were tested in this study: HKUST-1, IRMOF-1, MgMOF-74, MOF-177, MOF-801, NU-100, NU-125, UIO-66, and ZIF-8. When measuring Henry's law constant, the minimum R squared number was set to 0.9. Four of the nine MOFs have the acceptable Henry's regime within a certain trace gas composition which makes them potential applicants for the electronic nose that may be used to diagnose disease. So, within their appropriate regimes, we can use Henry's law constant measured to predict breath compositions. Figures 21–24 depict the relationship between overall adsorbed mass and mole fraction of acetone for the four MOFs that have appropriate Henry's regime. The plots demonstrate that the composition of CO_2 does not

affect Henry's coefficient of trace gases. It makes sense considering that air makes up the majority of the overall mass. If the convergency of our raspa simulations is not high enough, it will be hard to observe those subtle changes.

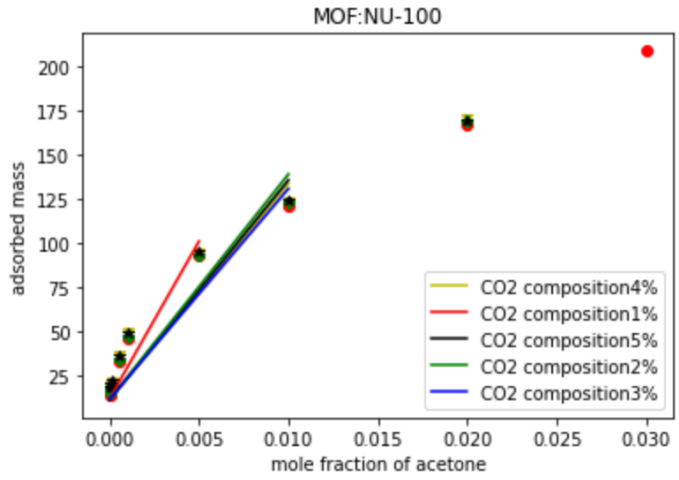

Figure 21 The Relationship between Total Adsorbed Mass and Mole Fraction of Acetone for NU-100

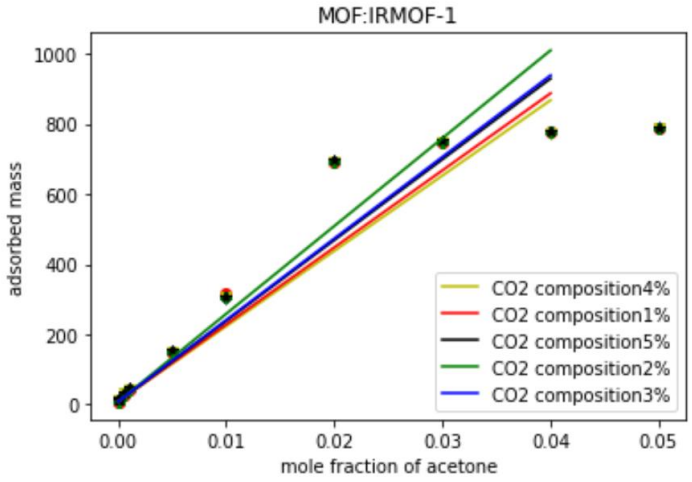

Figure 22 The Relationship between Total Adsorbed Mass and Mole Fraction of Acetone for IRMOF-1

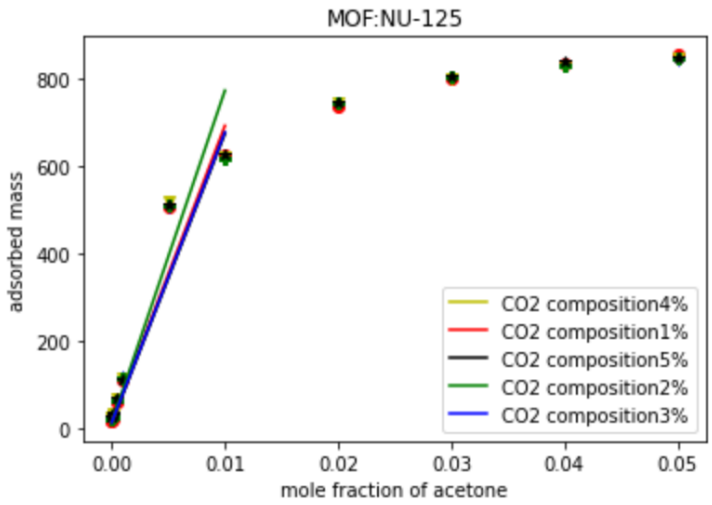

Figure 23 The Relationship between Total Adsorbed Mass and Mole Fraction of Acetone for NU-125

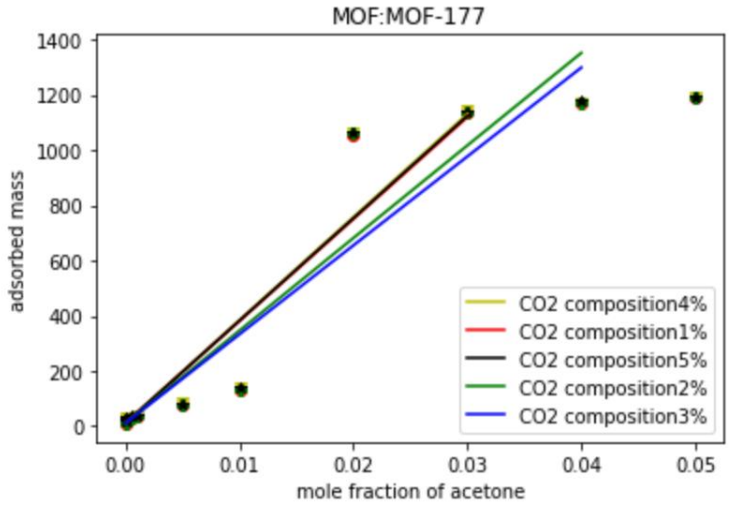

Figure 24 The Relationship between Total Adsorbed Mass and Mole Fraction of Acetone for MOF-177

4.0 Conclusion

We investigated the properties and applications of MOFs in three areas in this research.

First, we looked at how adsorption correlates with the number and types of defects. For relative pressures greater than 0.02, we greatly underestimate IPA loadings. The most likely explanation is that during the transference and reactivation, defects were introduced into the experimental samples. In comparison, our calculations overestimate N_2 loading for all pressures, and the most likely explanation is residual solvent in MOF. The standard UFF potential has been modified to capture hydrogen bonds, and formate is the most likely capping group.

Second, we used the QuickFF to generate new forcefields for both pristine UiO-66 and 17% defective UiO-66. The potential was validated using bulk modulus calculations, relaxation, and NVT simulations.

Third, we investigated one use of MOFs for the development of an electronic nose, a device designed to identify the composition of complex gas mixtures. Four of the nine screened MOFs have the acceptable Henry's regime within a certain gas composition. NU-100, IRMOF-1, NU-125, and MOF-177 are the four MOFs. They are potential applicants for the electronic nose that may be used to diagnose disease.

5.0 Publications

1. Lin Li, Christopher S. Ewing, Mona Abdelgaid, Sudesna Banerjee, Richard B. Garza, Robert Hacku, Nathan D. Hess, Sungil Hong, Meiirbek Islamov, Lauren L. Luciani, Stefanos Papadopoulos, Christopher Parker, Riddhesh A. Patel, Ritesh Pawar, Miranda H. Poklar, Maya Salem, Fathima Shabnam, Priyanka B. Shukla, Sai K. Vena, Huiran Wang, Rui Wang, Xin Wei, Fan Yang, and J. Karl Johnson, "Binding of CO and O on Low Symmetry Pt Clusters Supported on Amorphous Silica", Journal of Physical Chemistry C, under review (2021).
2. Yao An, Alfred Kleinhammes, Patrick Doyle, En-Yi Chen, Yan Song, Amanda J. Morris, Bradley Gibbons, Meng Cai, J. Karl Johnson, Priyanka B. Shukla, Minh Nguyen Vo, Xin Wei, Christopher E. Wilmer, Jonathan P. Ruffley, Liangliang Huang, Trenton M. Tovar, John J. Mahle, Christopher J. Karwacki, and Yue Wu, "In-situ NMR Investigation of Molecular Adsorption and Kinetics in MOF UiO-66", Journal of Physical Chemistry Letters, 12, 892-899 (2021). DOI: 10.1021/acs.jpclett.0c03504
3. Jacob J. Wardzala, Jonathan P. Ruffley, Isabella Goodenough, Allie M. Schmidt, Priyanka B. Shukla, Xin Wei, Abhishek Bagusetty, Mattheus De Souza, Prasenjit Das, Dorian J. Thompson, Christopher J. Karwacki, Christopher E. Wilmer, Eric Borguet, Nathaniel L. Rosi, and J. Karl Johnson "Modeling of Diffusion of Acetone in UiO-66", Journal of Physical Chemistry C, 124, 52, 28469-28478 / (2020). DOI: 10.1021/acs.jpcc.0c07040

Appendix A QuickFF Potentials

Appendix A.1 Potential Developed using QuickFF for Pristine UiO-66

```
# BONDHARM
#---------
BONDHARM:UNIT  K kjmol/A**2
BONDHARM:UNIT  R0 A

BONDHARM:PARS     C3_c2     C3_c2  4.0589245623e+03  1.3900238449e+00
BONDHARM:PARS     C3_c2     C3_c3  3.7929315942e+03  1.4043481343e+00
BONDHARM:PARS  C3_c1_o2     C3_c3  2.5780834839e+03  1.4956685751e+00
BONDHARM:PARS     C3_c2      H1_c  3.2337066495e+03  1.0915706820e+00
BONDHARM:PARS  C3_c1_o2    O2_czr  5.2973361246e+03  1.2772045342e+00
BONDHARM:PARS      H1_o    O4_zr3  4.8462405607e+03  9.6628116621e-01
BONDHARM:PARS    O2_czr  ZR12_o8_zr4  7.3919141084e+02  2.2209978615e+00
BONDHARM:PARS    O4_zr3  ZR12_o8_zr4  6.0090289278e+02  2.5816421382e+00
BONDHARM:PARS    O3_zr3  ZR12_o8_zr4  1.3154769771e+03  2.1236148141e+00

# BENDAHARM
#----------
BENDAHARM:UNIT  K kjmol/rad**2
BENDAHARM:UNIT  THETA0 deg

BENDAHARM:PARS     C3_c2     C3_c2      H1_c  2.3365745398e+02  1.2157825900e+02
BENDAHARM:PARS     C3_c3     C3_c2      H1_c  2.5855447315e+02  1.1848340850e+02
BENDAHARM:PARS     C3_c2     C3_c2     C3_c3  5.6924320918e+02  1.2014986850e+02
BENDAHARM:PARS     C3_c3  C3_c1_o2    O2_czr  6.1751003003e+02  1.1917076405e+02
BENDAHARM:PARS    O2_czr  C3_c1_o2    O2_czr  6.5332140589e+02  1.2039634243e+02
BENDAHARM:PARS  C3_c1_o2     C3_c3     C3_c2  4.0157134866e+02  1.2028673525e+02
BENDAHARM:PARS     C3_c2     C3_c3     C3_c2  5.1895131418e+02  1.1968687100e+02
BENDAHARM:PARS  C3_c1_o2    O2_czr  ZR12_o8_zr4  1.0837951462e+02  1.5482403605e+02
BENDAHARM:PARS      H1_o    O4_zr3  ZR12_o8_zr4  1.6052491561e+01  1.1590638072e+02
BENDAHARM:PARS  ZR12_o8_zr4    O4_zr3  ZR12_o8_zr4  2.5205513154e+02  7.7650494700e+01
BENDAHARM:PARS    O2_czr  ZR12_o8_zr4    O2_czr  2.5013674368e+02  1.0309462322e+02
BENDAHARM:PARS    O2_czr  ZR12_o8_zr4    O4_zr3  1.4370787857e+02  8.0918644879e+01
BENDAHARM:PARS    O4_zr3  ZR12_o8_zr4    O4_zr3  5.0967361024e+02  1.5206545468e+02
BENDAHARM:PARS    O2_czr  ZR12_o8_zr4    O3_zr3  2.8622224495e+01  4.2717599822e+01
BENDAHARM:PARS    O3_zr3  ZR12_o8_zr4    O4_zr3  9.7429212309e+02  8.6742397831e+01
BENDAHARM:PARS    O3_zr3  ZR12_o8_zr4    O3_zr3  3.9570494392e+02  1.0865134989e+02
```

```
# TORSION
#--------
TORSION:UNIT  A kjmol
TORSION:UNIT  PHI0 deg

TORSION:PARS     C3_c3     C3_c2     C3_c2     C3_c3  2 3.2864426706e+01  0.0000000000e+00
TORSION:PARS     C3_c3     C3_c2     C3_c2      H1_c  2 3.3840086388e+01  0.0000000000e+00
TORSION:PARS      H1_c     C3_c2     C3_c2      H1_c  2 1.7075028187e+01  0.0000000000e+00
TORSION:PARS  C3_c1_o2     C3_c3     C3_c2     C3_c2  2 4.0228047137e+01  0.0000000000e+00
TORSION:PARS  C3_c1_o2     C3_c3     C3_c2      H1_c  2 1.7970886655e+01  0.0000000000e+00
TORSION:PARS     C3_c2     C3_c2     C3_c3     C3_c2  2 3.0034784195e+01  0.0000000000e+00
TORSION:PARS     C3_c2     C3_c3     C3_c2      H1_c  2 2.7083593774e+01  0.0000000000e+00
TORSION:PARS     C3_c2     C3_c3  C3_c1_o2    O2_czr  2 3.5561208322e+00  0.0000000000e+00
TORSION:PARS     C3_c3  C3_c1_o2    O2_czr  ZR12_o8_zr4  2 1.2235367170e+01  0.0000000000e+00
TORSION:PARS    O2_czr  C3_c1_o2    O2_czr  ZR12_o8_zr4  2 5.1045168819e+00  0.0000000000e+00


# OOPDIST
#--------
OOPDIST:UNIT  K kjmol/A**2
OOPDIST:UNIT  D0 A

OOPDIST:PARS     C3_c2     C3_c3      H1_c     C3_c2  1.6346054972e+02  1.0848659971e-03
OOPDIST:PARS     C3_c3    O2_czr    O2_czr  C3_c1_o2  1.4563225322e+03  2.6387154697e-02
OOPDIST:PARS  C3_c1_o2     C3_c2     C3_c2     C3_c3  2.1978506272e+02  1.0089222939e-01
```

```
# Cross
Cross:UNIT  KSS kjmol/angstrom**2
Cross:UNIT  KBS0 kjmol/(angstrom*rad)
Cross:UNIT  KBS1 kjmol/(angstrom*rad)
Cross:UNIT  R0 angstrom
Cross:UNIT  R1 angstrom
Cross:UNIT  THETA0 deg
Cross:PARS     C3_c2     C3_c2      H1_c   3.8417911653e+01   7.3674027486e+01   1.0770950888e+02  1.3900238449e+00
1.0915706820e+00  1.2157825900e+02
Cross:PARS     C3_c3     C3_c2      H1_c   5.6963182212e+01   6.2572542387e+01   1.5015271626e+02  1.4043481343e+00
1.0915706820e+00  1.1848340850e+02
Cross:PARS     C3_c2     C3_c2     C3_c3   5.2023712510e+02   8.5979424968e+01   5.0041599839e+01  1.3900238449e+00
1.4043481343e+00  1.2014986850e+02
Cross:PARS     C3_c3  C3_c1_o2    O2_czr   4.0846232227e+02   1.6706092545e+02   4.1745220562e+02  1.4956685751e+00
1.2772045342e+00  1.1917076405e+02
Cross:PARS    O2_czr  C3_c1_o2    O2_czr   8.4675049017e+02   4.0099233265e+02   4.0099233265e+02  1.2772045342e+00
1.2772045342e+00  1.2039634243e+02
Cross:PARS  C3_c1_o2     C3_c3     C3_c2   3.0410086288e+02   1.3361276255e+02   8.5381301866e+01  1.4956685751e+00
1.4043481343e+00  1.2028673525e+02
Cross:PARS     C3_c2     C3_c3     C3_c2   5.3495554138e+02   2.9621902423e+01   2.9621902423e+01  1.4043481343e+00
1.4043481343e+00  1.1968687100e+02
Cross:PARS  C3_c1_o2    O2_czr  ZR12_o8_zr4   3.3968534792e+02   6.5230170983e+00   6.2320300406e+01  1.2772045342e+00
2.2209978615e+00  1.5482403605e+02
Cross:PARS      H1_o    O4_zr3  ZR12_o8_zr4  -3.1713101870e+00   1.6538044791e+02  -7.5359069262e+01  9.6628116621e-01
2.5816421382e+00  1.1590638072e+02
Cross:PARS  ZR12_o8_zr4    O4_zr3  ZR12_o8_zr4   3.1554703914e+02  -6.1651934288e+01  -6.1651934288e+01  2.5816421382e+0
2.5816421382e+00  7.7650494700e+01
Cross:PARS  ZR12_o8_zr4    O3_zr3  ZR12_o8_zr4   4.5469303497e+02   0.0000000000e+00   0.0000000000e+00  2.1236148141e+0
2.1236148141e+00  7.9174377511e+01
Cross:PARS    O2_czr  ZR12_o8_zr4    O2_czr   1.0997204906e+02   9.6368251683e+01   9.6368251683e+01  2.2209978615e+00
2.2209978615e+00  1.0309462322e+02
Cross:PARS    O2_czr  ZR12_o8_zr4    O4_zr3   7.3272081548e+01   9.4279412103e+01   1.1124880113e+02  2.2209978615e+00
2.5816421382e+00  8.0918644879e+01
Cross:PARS    O4_zr3  ZR12_o8_zr4    O4_zr3   5.1104575538e+01  -1.3320468874e+02  -1.3320468874e+02  2.5816421382e+00
2.5816421382e+00  1.5206545468e+02
Cross:PARS    O2_czr  ZR12_o8_zr4    O3_zr3   1.3149588196e+02   2.5023336895e+01   3.4719957816e+01  2.2209978615e+00
2.1236148141e+00  4.2717599822e+01
Cross:PARS    O3_zr3  ZR12_o8_zr4    O4_zr3  -2.6894651907e+00   5.7278362013e+01  -3.9230393090e+01  2.1236148141e+00
2.5816421382e+00  8.6742397831e+01
Cross:PARS    O3_zr3  ZR12_o8_zr4    O3_zr3   2.4001160562e+02   1.0407643067e+00   1.0407643067e+00  2.1236148141e+00
2.1236148141e+00  1.0865134989e+02
```

Appendix A.2 Potential Developed using QuickFF for UiO-66 with 17% Defects

```
# BONDHARM
#---------
BONDHARM:UNIT  K kjmol/A**2
BONDHARM:UNIT  R0 A

BONDHARM:PARS     C3_c2     C3_c2  4.0008433239e+03  1.3939803124e+00
BONDHARM:PARS     C3_c2     C3_c3  3.7517238773e+03  1.4082406805e+00
BONDHARM:PARS  C3_c1_o2     C3_c3  2.5664001076e+03  1.4950651294e+00
BONDHARM:PARS     C3_c2      H1_c  3.2861310371e+03  1.0856122346e+00
BONDHARM:PARS     C3_o2      H1_c  2.9810353349e+03  1.1063390969e+00
BONDHARM:PARS  C3_c1_o2    O2_czr  5.2038785547e+03  1.2815000820e+00
BONDHARM:PARS     C3_o2    O2_czr  5.5108053936e+03  1.2747561318e+00
BONDHARM:PARS      H1_o    O4_zr3  4.8262000008e+03  9.6753690029e-01
BONDHARM:PARS    O2_czr  ZR12_o8_zr4  7.4459526664e+02  2.2236217026e+00
BONDHARM:PARS    O4_zr3  ZR12_o8_zr4  5.2291850534e+02  2.5584296942e+00
BONDHARM:PARS    O3_zr3  ZR12_o8_zr4  1.3699036915e+03  2.1208708672e+00


# BENDAHARM
#----------
BENDAHARM:UNIT  K kjmol/rad**2
BENDAHARM:UNIT  THETA0 deg

BENDAHARM:PARS     C3_c2     C3_c2      H1_c  2.2308371965e+02  1.2214578115e+02
BENDAHARM:PARS     C3_c3     C3_c2      H1_c  2.4945821930e+02  1.1831471335e+02
BENDAHARM:PARS     C3_c2     C3_c2     C3_c3  5.7785286519e+02  1.2007178733e+02
BENDAHARM:PARS     C3_c3  C3_c1_o2    O2_czr  6.1949348410e+02  1.1878927063e+02
BENDAHARM:PARS    O2_czr  C3_c1_o2    O2_czr  6.3736982732e+02  1.2096479495e+02
BENDAHARM:PARS  C3_c1_o2     C3_c3     C3_c2  4.0859138026e+02  1.2047451503e+02
BENDAHARM:PARS     C3_c2     C3_c3     C3_c2  5.2342993340e+02  1.1967505532e+02
BENDAHARM:PARS      H1_c     C3_o2    O2_czr  3.7518684712e+02  1.1748326776e+02
BENDAHARM:PARS    O2_czr     C3_o2    O2_czr  7.5761173598e+02  1.2223891887e+02
BENDAHARM:PARS  C3_c1_o2    O2_czr  ZR12_o8_zr4  1.4118350988e+02  1.5281012594e+02
BENDAHARM:PARS     C3_o2    O2_czr  ZR12_o8_zr4  1.9522076176e+02  1.5044813251e+02
BENDAHARM:PARS    O2_czr  ZR12_o8_zr4    O3_zr3  4.0665017366e+01  5.5271594915e+01
BENDAHARM:PARS    O3_zr3  ZR12_o8_zr4    O4_zr3  9.3243775760e+02  8.6798443593e+01
BENDAHARM:PARS    O3_zr3  ZR12_o8_zr4    O3_zr3  4.2960764224e+02  1.0877415976e+02
BENDAHARM:PARS    O2_czr  ZR12_o8_zr4    O2_czr  2.6486410433e+02  1.0350010275e+02
BENDAHARM:PARS    O2_czr  ZR12_o8_zr4    O4_zr3  1.4911344902e+02  8.2528190999e+01
BENDAHARM:PARS    O4_zr3  ZR12_o8_zr4    O4_zr3  2.5568398276e+02  1.5153427025e+02
```

```
# BENDCOS
#--------
BENDCOS:UNIT  A kjmol
BENDCOS:UNIT  PHI0 deg

BENDCOS:PARS      H1_o    O4_zr3  ZR12_o8_zr4  1 2.1584836359e+02  1.8000000000e+02

# TORSION
#--------
TORSION:UNIT  A kjmol
TORSION:UNIT  PHI0 deg

TORSION:PARS     C3_c3     C3_c2     C3_c2     C3_c3  2 3.4091382920e+01  0.0000000000e+00
TORSION:PARS     C3_c3     C3_c2     C3_c2      H1_c  2 3.2008871180e+01  0.0000000000e+00
TORSION:PARS      H1_c     C3_c2     C3_c2      H1_c  2 1.6569432139e+01  0.0000000000e+00
TORSION:PARS  C3_c1_o2     C3_c3     C3_c2      H1_c  2 1.6874009499e+01  0.0000000000e+00
TORSION:PARS  C3_c1_o2     C3_c3     C3_c2     C3_c2  2 4.2341037785e+01  0.0000000000e+00
TORSION:PARS     C3_c2     C3_c3     C3_c2      H1_c  2 2.3849396595e+01  0.0000000000e+00
TORSION:PARS     C3_c2     C3_c2     C3_c3     C3_c2  2 3.1075498056e+01  0.0000000000e+00
TORSION:PARS     C3_c2     C3_c3  C3_c1_o2    O2_czr  2 1.0348351969e+01  0.0000000000e+00
TORSION:PARS     C3_c3  C3_c1_o2    O2_czr  ZR12_o8_zr4  2 1.2143960165e+01  0.0000000000e+00
TORSION:PARS    O2_czr  C3_c1_o2    O2_czr  ZR12_o8_zr4  2 5.7228393668e+00  0.0000000000e+00
TORSION:PARS    O2_czr     C3_o2    O2_czr  ZR12_o8_zr4  2 1.0853024758e+01  0.0000000000e+00
TORSION:PARS      H1_c     C3_o2    O2_czr  ZR12_o8_zr4  2 8.1696045205e+00  0.0000000000e+00

# OOPDIST
#--------
OOPDIST:UNIT  K kjmol/A**2
OOPDIST:UNIT  D0 A

OOPDIST:PARS     C3_c2     C3_c3      H1_c     C3_c2  1.5391593307e+02  2.6318103356e-03
OOPDIST:PARS     C3_c3    O2_czr    O2_czr  C3_c1_o2  1.3696118118e+03  2.3956046140e-02
OOPDIST:PARS  C3_c1_o2     C3_c2     C3_c2     C3_c3  1.6489669448e+02  1.3973052409e-01
OOPDIST:PARS      H1_c    O2_czr    O2_czr     C3_o2  1.4780517093e+03  4.2382449763e-03

# Cross
Cross:UNIT  KSS kjmol/angstrom**2
Cross:UNIT  KBS0 kjmol/(angstrom*rad)
Cross:UNIT  KBS1 kjmol/(angstrom*rad)
Cross:UNIT  R0 angstrom
Cross:UNIT  R1 angstrom
Cross:UNIT  THETA0 deg
Cross:PARS     C3_c2     C3_c2      H1_c   3.6121296987e+01   7.0425619778e+01   1.0379185200e+02  1.3939803124e+00  1.0856122346e+00
1.2214578115e+02
Cross:PARS     C3_c3     C3_c2      H1_c   5.6846903382e+01   6.1294108474e+01   1.5034914735e+02  1.4082406805e+00  1.0856122346e+00
1.1831471335e+02
Cross:PARS     C3_c2     C3_c2     C3_c3   5.2061771802e+02   8.1772892896e+01   4.2932452335e+01  1.3939803124e+00  1.4082406805e+00
1.2007178733e+02
Cross:PARS     C3_c3  C3_c1_o2    O2_czr   4.0679160372e+02   1.6633825503e+02   4.2148396904e+02  1.4950651294e+00  1.2815000820e+00
1.1878927063e+02
Cross:PARS    O2_czr  C3_c1_o2    O2_czr   8.3182275449e+02   3.8970653060e+02   3.8970653060e+02  1.2815000820e+00  1.2815000820e+00
1.2096479495e+02
Cross:PARS  C3_c1_o2     C3_c3     C3_c2   3.0385716949e+02   1.3427244506e+02   9.0287441115e+01  1.4950651294e+00  1.4082406805e+00
1.2047451503e+02
Cross:PARS     C3_c2     C3_c3     C3_c2   5.3437078776e+02   2.8331241085e+01   2.8331241085e+01  1.4082406805e+00  1.4082406805e+00
1.1967505532e+02
Cross:PARS      H1_c     C3_o2    O2_czr   2.2641843167e+02   1.2107026001e+02   3.1431283758e+02  1.1063390969e+00  1.2747561318e+00
1.1748326776e+02
Cross:PARS    O2_czr     C3_o2    O2_czr   9.0283689181e+02   2.6636451522e+02   2.6636451522e+02  1.2747561318e+00  1.2747561318e+00
1.2223891887e+02
```

```
Cross:PARS  C3_c1_o2    O2_czr  ZR12_o8_zr4   3.4539361765e+02   1.3789789884e+01   6.3600970405e+01  1.2815000820e+00
2.2236217026e+00  1.5281012594e+02
Cross:PARS     C3_o2    O2_czr  ZR12_o8_zr4   3.2614240493e+02   2.1649099480e+01   8.5199170859e+01  1.2747561318e+00
2.2236217026e+00  1.5044813251e+02
Cross:PARS      H1_o    O4_zr3  ZR12_o8_zr4   1.0105187910e+02  -2.7967547719e+00   6.7924749123e+00  9.6753690029e-01
2.5584296942e+00  -5.7295779513e+01
Cross:PARS  ZR12_o8_zr4    O4_zr3  ZR12_o8_zr4   2.4785633096e+02   0.0000000000e+00   0.0000000000e+00  2.5584296942e+00
2.5584296942e+00  7.8483372683e+01
Cross:PARS  ZR12_o8_zr4    O3_zr3  ZR12_o8_zr4   4.6429776481e+02   0.0000000000e+00   0.0000000000e+00  2.1208708672e+00
2.1208708672e+00  7.7696247171e+01
Cross:PARS    O2_czr  ZR12_o8_zr4    O3_zr3   1.2996783339e+02   1.9010184719e+01   4.1562737103e+01  2.2236217026e+00
2.1208708672e+00  5.5271594915e+01
Cross:PARS    O3_zr3  ZR12_o8_zr4    O4_zr3   1.6510561478e+01   1.2143967967e+02  -8.1854034423e+01  2.1208708672e+00
2.5584296942e+00  8.6798443593e+01
Cross:PARS    O3_zr3  ZR12_o8_zr4    O3_zr3   2.3647235509e+02  -1.8002542282e+01  -1.8002542282e+01  2.1208708672e+00
2.1208708672e+00  1.0877415976e+02
Cross:PARS    O2_czr  ZR12_o8_zr4    O2_czr   1.0683219835e+02   9.1624932257e+01   9.1624932257e+01  2.2236217026e+00
2.2236217026e+00  1.0350010275e+02
Cross:PARS    O2_czr  ZR12_o8_zr4    O4_zr3   6.9805419800e+01   8.5317969978e+01   9.9316700176e+01  2.2236217026e+00
2.5584296942e+00  8.2528190999e+01
Cross:PARS    O4_zr3  ZR12_o8_zr4    O4_zr3  -9.9221375109e+00  -9.8812627135e+01  -9.8812627135e+01  2.5584296942e+00
2.5584296942e+00  1.5153427025e+02
```

Bibliography

1.Shearer, G. C.; Chavan, S.; Bordiga, S.; Svelle, S.; Olsbye, U.; Lillerud, K. P., Defect Engineering: Tuning the Porosity and Composition of the Metal–Organic Framework UiO-66 via Modulated Synthesis. *Chemistry of Materials* **2016,** *28* (11), 3749-3761.

2.Shearer, G. C.; Chavan, S.; Ethiraj, J.; Vitillo, J. G.; Svelle, S.; Olsbye, U.; Lamberti, C.; Bordiga, S.; Lillerud, K. P., Tuned to Perfection: Ironing Out the Defects in Metal–Organic Framework UiO-66. *Chem. Mater.* **2014,** *26* (14), 4068-4071.

3.Katz, M. J.; Brown, Z. J.; Colón, Y. J.; Siu, P. W.; Scheidt, K. A.; Snurr, R. Q.; Hupp, J. T.; Farha, O. K., A Facile Synthesis of UiO-66, UiO-67 and Their Derivatives. *Chemical Communications* **2013,** *49* (82), 9449-9451.

4.Vandichel, M.; Hajek, J.; Vermoortele, F.; Waroquier, M.; De Vos, D. E.; Van Speybroeck, V., Active Site Engineering in UiO-66 Type Metal–Organic Frameworks by Intentional Creation of Defects: a Theoretical Rationalization. *CrystEngComm* **2015,** *17* (2), 395-406.

5.DeStefano, M. R.; Islamoglu, T.; Garibay, S. J.; Hupp, J. T.; Farha, O. K., Room-Temperature Synthesis of UiO-66 and Thermal Modulation of Densities of Defect Sites. *Chemistry of Materials* **2017,** *29* (3), 1357-1361.

6.Peterson, G. W.; Destefano, M. R.; Garibay, S. J.; Ploskonka, A.; McEntee, M.; Hall, M.; Karwacki, C. J.; Hupp, J. T.; Farha, O. K., Optimizing Toxic Chemical Removal through Defect-Induced UiO66-NH2Metal−Organic Framework. *Chem. - Eur. J.* **2017,** *23 (63)*, 15913−15916.

7.An, Y.; Kleinhammes, A.; Doyle, P.; Chen, E.-Y.; Song, Y.; Morris, A. J.; Gibbons, B.; Cai, M.; Johnson, J. K.; Shukla, P. B.; Vo, M. N.; Wei, X.; Wilmer, C. E.; Ruffley, J. P.; Huang, L.; Tovar, T. M.; Mahle, J. J.; Karwacki, C. J.; Wu, Y., In Situ Nuclear Magnetic Resonance Investigation of Molecular Adsorption and Kinetics in Metal–Organic Framework UiO-66. *J. Phys. Chem. Lett.* **2021,** *12* (2), 892-899.

8.Bristow, J. K.; Svane, K. L.; Tiana, D.; Skelton, J. M.; Gale, J. D.; Walsh, A., Free Energy of Ligand Removal in the Metal-Organic Framework UiO-66. *The journal of physical chemistry. C, Nanomaterials and interfaces* **2016,** *120* (17), 9276-9281.

9.Manz, T. A.; Limas, N. G., Introducing DDEC6 Atomic Population Analysis: Part 1. Charge Partitioning Theory and Methodology. *RSC Advances* **2016,** *6* (53), 47771-47801.

10.Manz, T. A., Introducing DDEC6 Atomic Population Analysis: Part 3. Comprehensive Method to Compute Bond Orders. *RSC Advances* **2017,** *7* (72), 45552-45581.

11.Limas, N. G.; Manz, T. A., Introducing DDEC6 Atomic Population Analysis: Part 4. Efficient Parallel Computation of Net Atomic Charges, Atomic Spin Moments, Bond Orders, and More. *RSC Advances* **2018,** *8* (5), 2678-2707.

12.Limas, N. G.; Manz, T. A., Introducing DDEC6 Atomic Population Analysis: Part 2. Computed Results for a Wide Range of Periodic and Nonperiodic Materials. *RSC Advances* **2016,** *6* (51), 45727-45747.

13.Wilmer, C. E.; Kim, K. C.; Snurr, R. Q., An Extended Charge Equilibration Method. *J. Phys. Chem. Lett.* **2012,** *3* (17), 2506-2511.

14.Yang, D.; Ortuño, M. A.; Bernales, V.; Cramer, C. J.; Gagliardi, L.; Gates, B. C., Structure and Dynamics of Zr6O8 Metal–Organic Framework Node Surfaces Probed with Ethanol Dehydration as a Catalytic Test Reaction. *Journal of the American Chemical Society* **2018,** *140* (10), 3751-3759.

15.Vanduyfhuys, L.; Vandenbrande, S.; Wieme, J.; Waroquier, M.; Verstraelen, T.; V. Van Speybroeck, Extension of the QuickFF force field protocol for an improved accuracy of structural, vibrational, mechanical and thermal properties of metal–organic frameworks. *J. Comput. Chem* **J. Comput. Chem,** *39* (16), 999-1011.

16.Wardzala, J. J.; Ruffley, J. P.; Goodenough, I.; Schmidt, A. M.; Shukla, P. B.; Wei, X.; Bagusetty, A.; De Souza, M.; Das, P.; Thompson, D. J.; Karwacki, C. J.; Wilmer, C. E.; Borguet, E.; Rosi, N. L.; Johnson, J. K., Modeling of Diffusion of Acetone in UiO-66. *The Journal of Physical Chemistry C* **2020,** *124* (52), 28469-28478.

17.Vanduyfhuys, L.; Vandenbrande, S.; Verstraelen, T.; Schmid, R.; Waroquier, M.; Van Speybroeck, V., QuickFF: A program for a quick and easy derivation of force fields for metal-organic frameworks from ab initio input. *J Comput Chem* **2015,** *36* (13), 1015-27.

18.Vanduyfhuys, L.; Vandenbrande, S.; Wieme, J.; Waroquier, M.; Verstraelen, T.; Van Speybroeck, V., Extension of the QuickFF force field protocol for an improved accuracy of structural, vibrational, mechanical and thermal properties of metal-organic frameworks. *J Comput Chem* **2018,** *39* (16), 999-1011.

19.Day, B. A.; Wilmer, C. E., Genetic Algorithm Design of MOF-based Gas Sensor Arrays for CO2-in-Air Sensing. *Sensors* **2020,** *20* (3), 924.

20.Gustafson, J. A.; Wilmer, C. E., Computational Design of Metal–Organic Framework Arrays for Gas Sensing: Influence of Array Size and Composition on Sensor Performance. *The Journal of Physical Chemistry C* **2017,** *121* (11), 6033-6038.